Membrane action in reinforced concrete slabs

F. J. VECCHIO
Department of Civil Engineering, University of Toronto, 35 St. George Street, Toronto, Ont., Canada M5S 1A4

AND

K. TANG
Adjeleian, Allen and Rubeli Ltd., Consulting Engineers, 20 Eglinton Avenue W., Toronto, Ont., Canada M4R 1K8

Received August 2, 1989
Revised manuscript accepted March 13, 1990

The formation and influence of compressive membrane action in reinforced concrete slabs is discussed. An experimental program is described, in which two large-scale slab specimens were tested under concentrated midspan loads. One slab was restrained against lateral expansion at the ends, while the other was free to elongate. The laterally restrained specimen developed high axial compressive forces, which resulted in a significant increase in flexural stiffness and load capacity. A nonlinear analysis procedure was used to model specimen behaviour. The analysis method was found to adequately represent important second-order effects, and thus gave reasonably accurate predictions of load–deformation response and ultimate load.

Key words: analysis, concrete, deformation, load, membrane, reinforced, slabs, strength, tests.

La formation et l'influence des mouvements de compression de la membrane à l'intérieur des dalles de béton armé sont traitées dans cet article. Les auteurs décrivent un programme expérimental à l'intérieur duquel deux échantillons de dalle pleine grandeur sont soumis à des essais de charge concentrée au milieu. L'une des dalles est encastrée aux extrémités afin de prévenir la dilatation latérale, alors que l'autre était libre de tout mouvement. L'échantillon encastré a produit des forces de compression axiale élevées qui ont entraîné une importante augmentation de la rigidité à la flexion et de la capacité de charge. Une méthode d'analyse non linéaire a été utilisée afin de modéliser le comportement de l'échantillon. Cette méthode a permis de représenter de manière satisfaisante les effets de second ordre et d'obtenir des prévisions relativement fiables de la relation charge — déformation et de la charge ultime.

Mots clés : analyse, béton, déformation, charge, membrane, armé, dalles, résistance, essais.

[Traduit par la revue]

Can. J. Civ. Eng. **17**, 686–697 (1990)

Introduction

The structural aspects pertaining to the 1978 collapse of a warehouse structure in Niagara Falls were examined in a recent paper (Vecchio and Collins 1990). The collapsed structure was the Kimberley–Clark Warehouse building, a four-storey reinforced concrete structure with flat-slab floors supported on columns with capitals. Its floors were designed for a dead load of 4.8 kN/m^2 and a superimposed live load of 6.0 kN/m^2; thus the total design load was 10.8 kN/m^2. In time, the third floor of the building came to be used as a storage site for nickel materials. At the time of collapse, the total load imposed over several entire bays of the third floor was estimated to be in excess of 48 kN/m^2. It is a disputed issue as to whether overloading of the floor, or the effects of a fire burning directly beneath, caused collapse. Nevertheless, the floor demonstrated a factor of safety against collapse of 4.5 relative to the design loads. It was surmised that this high strength reserve was developed primarily through the influence of compressive membrane action in the slabs.

Analyses were conducted to determine the floor's theoretical load capacity (Vecchio and Collins 1990). A section of the third floor along an interior column line was represented as a plane frame structure, and was analyzed using the nonlinear analysis program TEMPEST (Vecchio 1987). The theoretical floor capacity determined, drawing heavily on the influence of second-order effects, was about 50 kN/m^2. Some doubts existed, however, regarding the accuracy of modelling two-way action using a plane frame representation. Appropriate three-dimensional analysis methods, which would adequately capture all the second-order influences considered critical to response in this case, were not available.

A test program was subsequently undertaken, in support of the theoretical analyses, to investigate compressive membrane action in slabs. Specific objectives were to observe the formation and influence of this behaviour, and to verify and further develop theoretical modelling techniques. Slab strip specimens were used in the test program to better isolate the influence of membrane action and to address the plane frame modelling assumption.

This paper discusses the details and results of the test program. The accuracy of current theoretical analysis procedures is also examined.

Membrane action

Consider the behaviour of a reinforced concrete slab under transverse load, shown in Fig. 1. As the slab deflects under load, the concrete on the tension face cracks and the reinforcement is stretched. Typically, the strains on the tension face will be considerably greater in magnitude than those on the compression face. The net tensile strain resulting at the slab mid-depth causes the slab to expand, producing outward horizontal displacements at the slab ends. The tendency to expand will be prevented, to some degree, by the lateral stiffness of supporting columns, beams, or walls. Adjoining slab panels will also

NOTE: Written discussion of this paper is welcomed and will be received by the Editor until February 28, 1991 (address inside front cover).

Printed in Canada / Imprimé au Canada

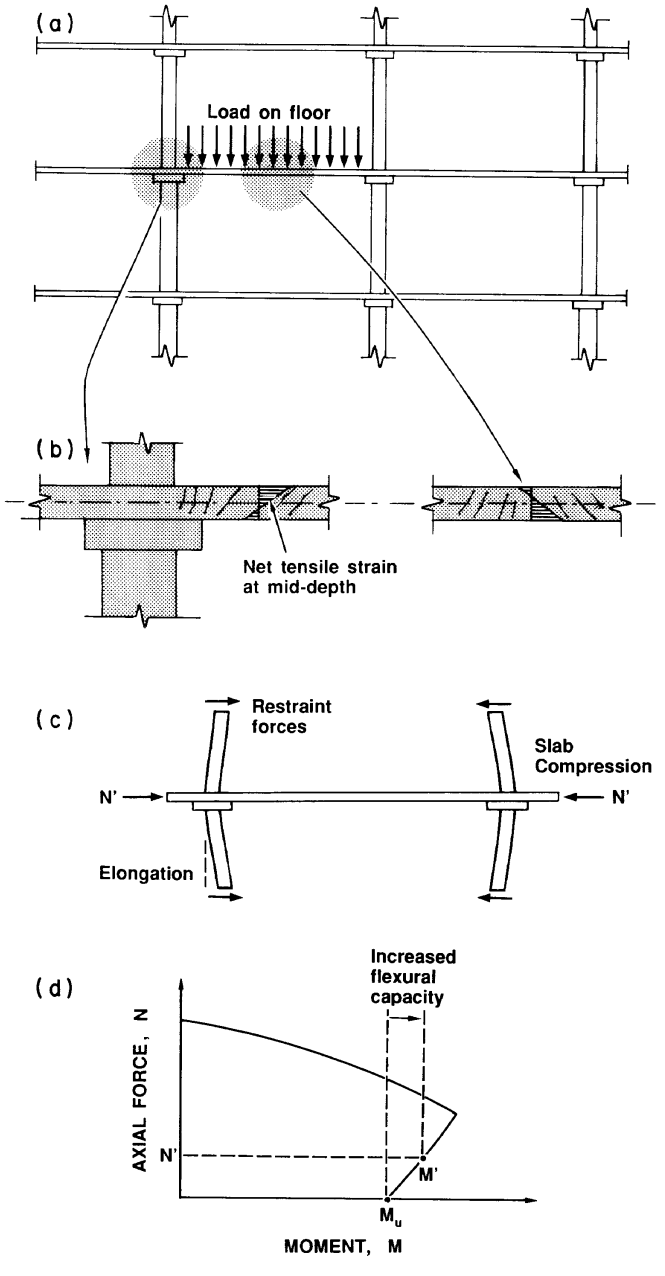

FIG. 1. Axial forces developed in laterally restrained slab: (*a*) slab subjected to transverse loading; (*b*) slab elongates upon cracking; (*c*) restrained elongation induces axial compression; (*d*) axial compression increases flexural capacity.

form an extremely stiff diaphragm which will oppose the expansion of the loaded slab. As a result, compressive membrane forces will be induced in the loaded slab owing to restrained expansion. The compressive forces, in turn, produce an increase in the nominal flexural capacity of the slab section. This mechanism is commonly known as membrane action and can lead to significant increases in the load-carrying capacity of a slab. At more advanced stages of deformation, the concrete may crush completely leaving only the reinforcement to act as a tensile net. This second-stage behaviour is termed catenary action.

Membrane action has long been noted in both full-scale and laboratory tests. The earliest observations were made by Westergaard and Slater (1921) in testing a number of full-scale slab panels, supported on four sides and loaded to ultimate capacity. The tests indicated that with increased slab deformation, a redistribution of moments and stresses took place. The ultimate load attained was larger, and in some cases much larger, than the known strength of beams with similar reinforcement ratios. At that time, a satisfactory account could not be made for the unexpectedly high strength exhibited by the slabs.

Perhaps the most dramatic demonstration of membrane action was made by Ockelston (1955). The floor slabs in a 10-year-old, three-storey reinforced concrete structure were intentionally loaded to destruction. The lightly reinforced two-way slab panels were 135 mm thick, 4.9 m by 4.1 m in plan, and bounded by main and secondary beams. The slabs were designed for a dead load of 3.2 kN/m^2 and a superimposed floor load of 3.4 kN/m^2. Upon gradual loading, the floor did not collapse until the total load reached 40.4 kN/m^2, representing a factor of safety of 6.1. Ockelston partly attributed this unexpected strength reserve to membrane action.

Christiansen (1963) later presented a method for analysis of membrane action in beams and one-way slabs with lateral restraint and uniformly distributed loading. Expressions were derived to estimate the magnitude of the membrane force induced in the slab. The outward movement of the slab was then accounted for by assuming it to be proportional to the membrane force and a function of the rigidity of adjoining members. A relative stiffness factor was required for the calculations and had to be estimated on the basis of experimental data. Given the membrane force, the ultimate load capacity could then be determined. Christiansen later expanded on the formulations to address rectangular two-way slabs.

Park (1965) also derived expressions to calculate the ultimate load of rectangular two-way slabs under uniform loading and with edges restrained against lateral movement. The equations, derived, based on Johansen's (1962) yield-line theory, represented a compressive membrane action using a rigid-plastic strip approximation and an empirical value for the deflection at ultimate load. Park showed from experiment that the maximum deflection at ultimate was in the range of 0.4 to 0.5 of the slab depth, regardless of the span-to-depth ratio. Park also demonstrated that to enforce membrane action in the panels of beam-slab floors, extra tie reinforcement should be placed continuously around the supporting beams.

Hopkins and Park (1971) further investigated membrane behaviour by designing and testing a quarter-scale nine-panel reinforced concrete slab-beam floor. The results were used to further assess previous formulations. Brotchie and Holley (1971), at the same time, tested 45 small-scale slab specimens. All the slabs tested were 381 mm square, and uniformly loaded. Simple expressions were derived to describe both compressive and tensile membrane effects, and the ultimate load corresponding to each. Important work in this area, leading to developments in design code specifications, was also undertaken by Kinnunnen and Nylander (1960) and by Hewitt and Batchelor (1975).

Most recently, Guice and Rhomberg (1988) reported on a test series involving 16 one-way slab strips under uniform loading. It was concluded that the compressive membrane action predicted by Park's formulations provided an upper bound to experimental flexural capacities, in some cases significantly overpredicting ultimate load. It was also determined that rotational restraint at the ends was essential to developing significant compressive membrane forces.

The studies described above relate primarily to behaviour at ultimate conditions and to predictions of load capacity. Few methods are discussed in the literature by which the complete load–deformation response of a slab influenced by membrane action can be accurately computed. The nonlinear finite element procedures being developed by researchers today certainly have the potential to do this. However, no such procedure has yet been shown to specifically address and adequately model this second-order behaviour in slabs.

Experimental program

The experimental program involved the testing of two large-scale slab strip specimens, loaded under monotonically increasing line loads applied at the midspan. The specimen configuration consisted of a 100 mm thick, 1500 mm wide slab strip built integral with two stub columns (see Fig. 2*a*). The column stubs were 200 × 200 mm in cross section, spaced 3075 mm apart on centres, and extended 750 mm below the slab and 350 mm above. A 400 mm square, 100 mm thick drop panel was provided at each column for punching shear resistance. Transverse edge beams were included at the ends of the slab strip to facilitate the desired support conditions. The total length of the slab specimen was 6.25 m (20.5 ft). The slab thickness and span dimensions represented a half-scale model of the Kimberley–Clark Warehouse floor.

The two specimens tested were identically designed, built, and tested, differing only in the support conditions imposed. For slab TV1, the end supports were allowed to displace horizontally; in slab TV2, the two ends were fixed against any horizontal displacements (see Fig. 2*b*). Thus, differences in the ability of each slab to resist applied transverse loads would be derived entirely from differences in the axial restraint forces induced. In both specimens, the slab ends were fixed against vertical deflection and the column bases were fixed against vertical and horizontal displacements but were free to rotate.

Details of the reinforcement provided in the slabs are given in Fig. 3. The top longitudinal reinforcement over the column supports consisted of No. 10 bars at 150 mm spacing, giving a reinforcement ratio of $\rho = 0.66\%$. The bottom longitudinal reinforcement at the midspan comprised of No. 10 bars at 300 mm spacing ($\rho = 0.33\%$). Transverse reinforcement in the same amounts was also provided. Thus, the reinforcement percentages and layouts used were essentially similar to those found in the third floor of the Kimberley–Clark Warehouse. The columns were reinforced with eight No. 15 longitudinal bars ($\rho = 4.0\%$), and with 8 mm double ties at 200 mm spacing. The clear cover provided was 10 mm for the slab and 20 mm for the columns.

The concrete used in casting the specimens was of 30 MPa nominal strength, with a 10 mm maximum size coarse aggregate. The two specimens were cast from separate batches and allowed to cure approximately 120 days before testing. The concrete properties were determined, at the time of testing, from 150 mm × 300 mm diameter cylinders. Cylinder compression tests were carried out on a servo-controlled stiff frame, using a stroke rate of 0.0033 mm/s. Tensile strengths were determined from split cylinder tests. Table 1 summarizes the concrete material properties determined, and a typical stress–strain curve is given in Fig. 4*a*.

The reinforcement used consisted of deformed bars of No. 10, No. 15, and 8 mm diameter designations. The material properties of the reinforcement, determined from coupon tests, are also given in Table 1. Shown in Fig. 4*b* are typical stress–strain curves obtained for each of the reinforcement bar types. Note that for the No. 10 bars, which constituted the main reinforcement for the slabs, no distinct yield plateau was found. The yield stress and yield strain were obtained using the 0.2% offset method.

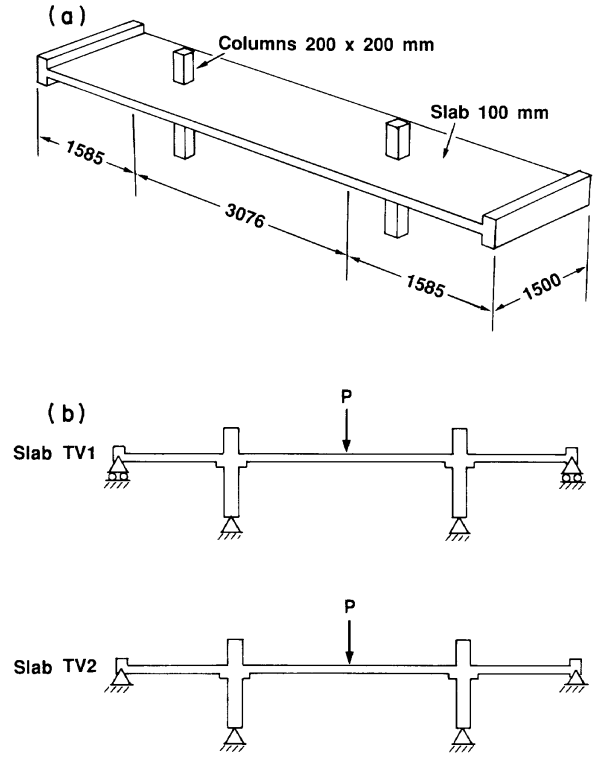

FIG. 2. General overview of slab strip specimens: (*a*) slab strip configuration; (*b*) loading and support conditions.

The test setup devised for loading the slab specimens is illustrated in Fig. 5. The columns were supported on prefabricated pin-roller assemblies in order to simulate a pin-joint condition at the base of the columns. The bottom of the supports rested on roller-base assemblies and were free to move horizontally. A 350 kN capacity servo-controlled force actuator was used to connect between the two roller bases, maintaining zero relative displacement between the two pins at all times. At the slab ends, two 25 mm diameter steel tie-rods anchored to the strong floor were used to restrain each edge beam against vertical displacement.

For slab TV2, the objective was to maintain the relative horizontal displacement of the slab ends at zero. This was achieved by using a 1000 kN capacity servo-controlled force actuator mounted horizontally and bearing on the edge beam at one end of the slab. The actuator was then attached to a reaction frame which connected to the strong floor. At the other end, horizontal movement was restricted by bearing against a strong wall. The actuator was then employed in displacement control mode to maintain zero net elongation of the slab. The setup for slab TV1 did not require use of the 1000 kN actuator.

Vertical loads were applied at the midspan of the slabs by two 250 kN capacity servo-controlled actuators. A heavy steel spreader beam, on a 150 mm wide steel bearing plate, was

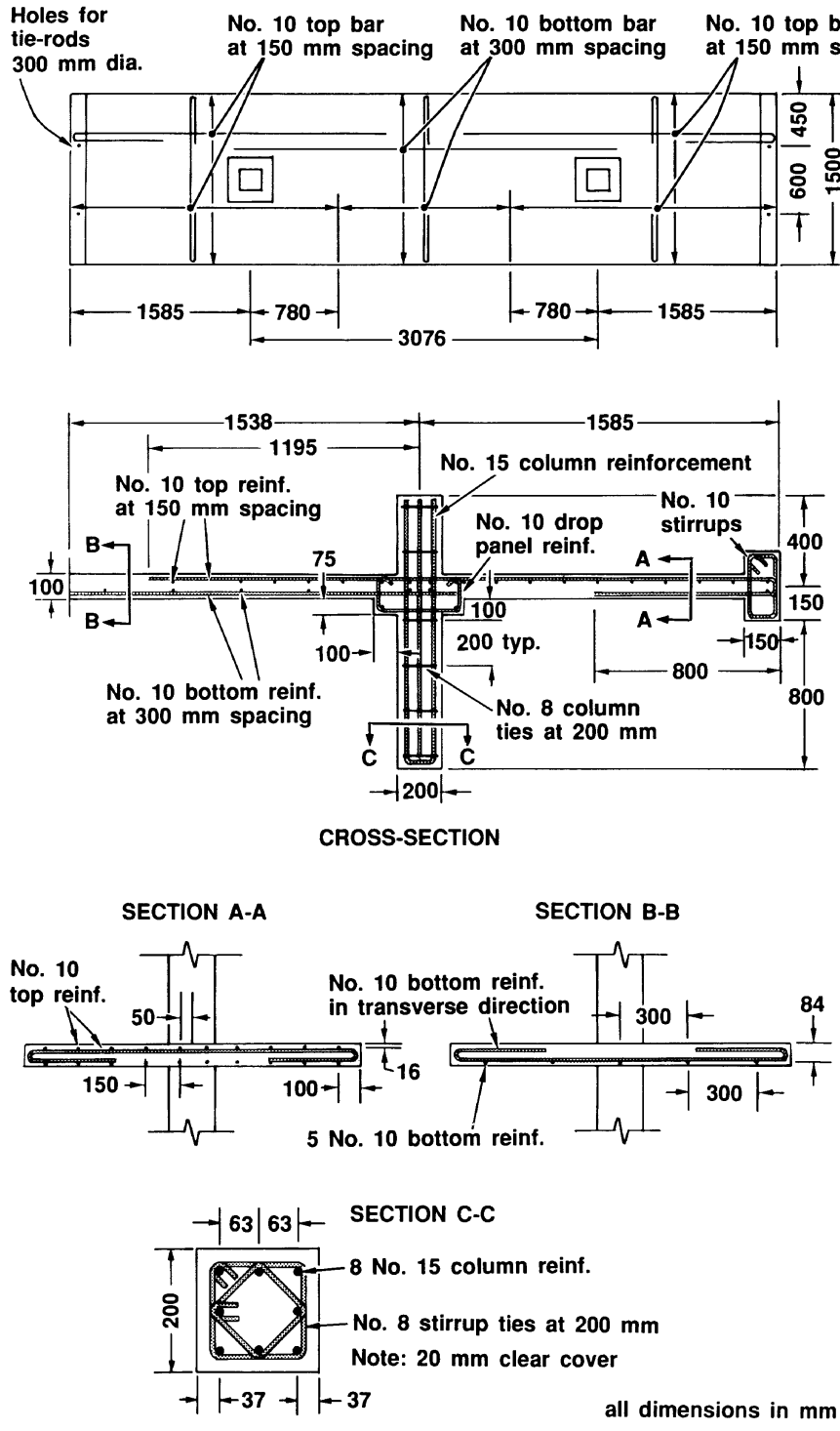

FIG. 3. Specimen reinforcement details.

TABLE 1. Material properties of concrete and reinforcement

	Concrete				Reinforcement				
Specimen	f'_c (MPa)	f_{ct} (MPa)	ε_0 ($\times 10^{-3}$)	E_c (MPa)	Bar size	A_s (mm^2)	f_y (MPa)	f_u (MPa)	E_s (MPa)
TV1	29.7	3.2	1.95	30 500	No. 10	100	454	649	
TV2	30.2	3.6	1.99	32 200	No. 15	200	484	646	201 700
					8 mm	51	607	607	202 500

used to convert the two actuator point loads into a uniform line load. The actuators reacted against a loading frame which was also connected to the strong floor.

The applied loads and reaction forces were monitored by load cells built into the actuators. As well, load cells were included on each of the tie-rods providing vertical restraint at the slab ends. Displacement transducers (LVDTs) were used to monitor vertical deflections of the slab at various points along its length. As well, horizontal deflections were similarly monitored at the column ends, column–slab joints, and slab ends. To measure average curvature and axial elongation along the slabs, demountable mechanical strain gauges were used on a continuous 200 mm grid. Electrical resistance strain gauges, applied onto the reinforcing bars at various locations, gave a measure of rebar stresses. All instrument readings were continuously monitored and recorded using a computer-controlled data acquisition system.

The specimens were subjected to monotonically increasing loads, applied in a displacement-controlled mode. The two 250-kN capacity actuators were coupled such that similar displacement of each actuator was maintained at all times.

Test observations

Each of the two test specimens developed minor shrinkage cracking prior to testing. In slab TV1, three cracks, each of less than 0.05 mm width, developed over a partial width of the underside of the slab at the midspan, and one crack of 0.05 mm width developed fully across the slab near a column. In slab TV2, initial cracks of similar width were also found on the underside of the slab at the midspan and quarter-span points.

During loading of slab TV1, first evidence of flexural cracking at the midspan was observed at a load of 15 kN and was accompanied by a decrease in load–deformation stiffness. As the loads increased thereafter, transverse flexural cracks progressively formed near both column supports and at the midspan. At a load of 50 kN, yielding of the bottom reinforcement at the midspan was detected, and crack widths in this region exceeded 0.70 mm. Radial cracks began to form on the top surface of the slab, around the columns, at a load of 60 kN. No degradation in the stiffness of the load–deformation response was evident at this time, however. At an applied load of 63 kN, a sudden failure of the specimen occurred owing to a suspected malfunction of the servo-valve on one of the two loading actuators. The actuator instantly applied full stroke, resulting in a brittle shear failure of the slab at the load application point. A view of the failed specimen is seen in Fig. 6*a*.

Slab TV2 exhibited an essentially linear load–deformation response well beyond the occurrence of first cracking. Initially, transverse cracks progressively formed at the midspan and column regions across the full width of the slab. Above 50 kN load, radial cracks began to form on the top surface of the slab near the columns. Yielding of the bottom reinforcement at the midspan was detected at a load of 66 kN, resulting in a perceptible decrease in the stiffness of the load–deformation response. Further decreases in stiffness occurred upon yielding of the top reinforcement near the columns, at a load of 85 kN. An ultimate load of 89.5 kN was attained, accompanied by a very ductile post-ultimate behaviour. Loading continued until, at a midspan deflection of 180 mm, rebars at the midspan ruptured (see Fig. 6*b*). It should be noted that the horizontal actuator at the slab end was required to apply compressive forces right up to failure, and thus catenary action was not achievable.

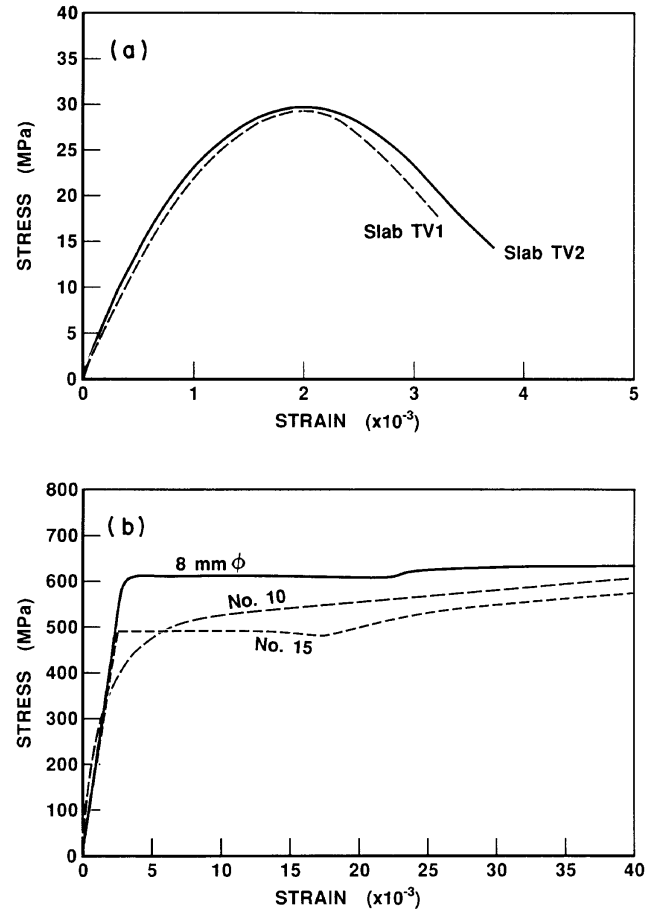

FIG. 4. Material stress–strain behaviour: (*a*) concrete; (*b*) reinforcement.

The measured slab deflections at midspan, relative to the column joints, are given in Fig. 7*a*. Only in slab TV1 is there a perceptible change in stiffness upon first cracking. In slab TV2, with axial compressive forces being developed in the slab, no such sharp transition occurs. In both specimens, however, pronounced degradation in stiffness accompanies yielding of the reinforcement. Initially, the deflection response of the two specimens are seen to be similar. However, at loads above 40 kN, the response of slab TV2 is seen to be significantly stiffer as the influence of the axial compression becomes evident. The post-ultimate behaviour of slab TV2 remains very ductile with little decrease in load capacity. For slab TV1, there is no indication in the deflection response that the ultimate load capacity was approached before failure occurred.

The relative horizontal deflection of the slab ends, for slab TV1, is shown in Fig. 7*b*. (The end deflections in slab TV2 were maintained at zero through the support conditions imposed.) In slab TV1, the relative end deflection accelerated after initial cracking and increased at a relatively constant rate thereafter. It should also be noted that zero relative end displacement in slab TV2 does not imply that no elongation of the slab occurred. In fact, the increase in arc length of the deflected slab allows for a significant net expansion to occur. As determined from mechanical strain measurements along the length

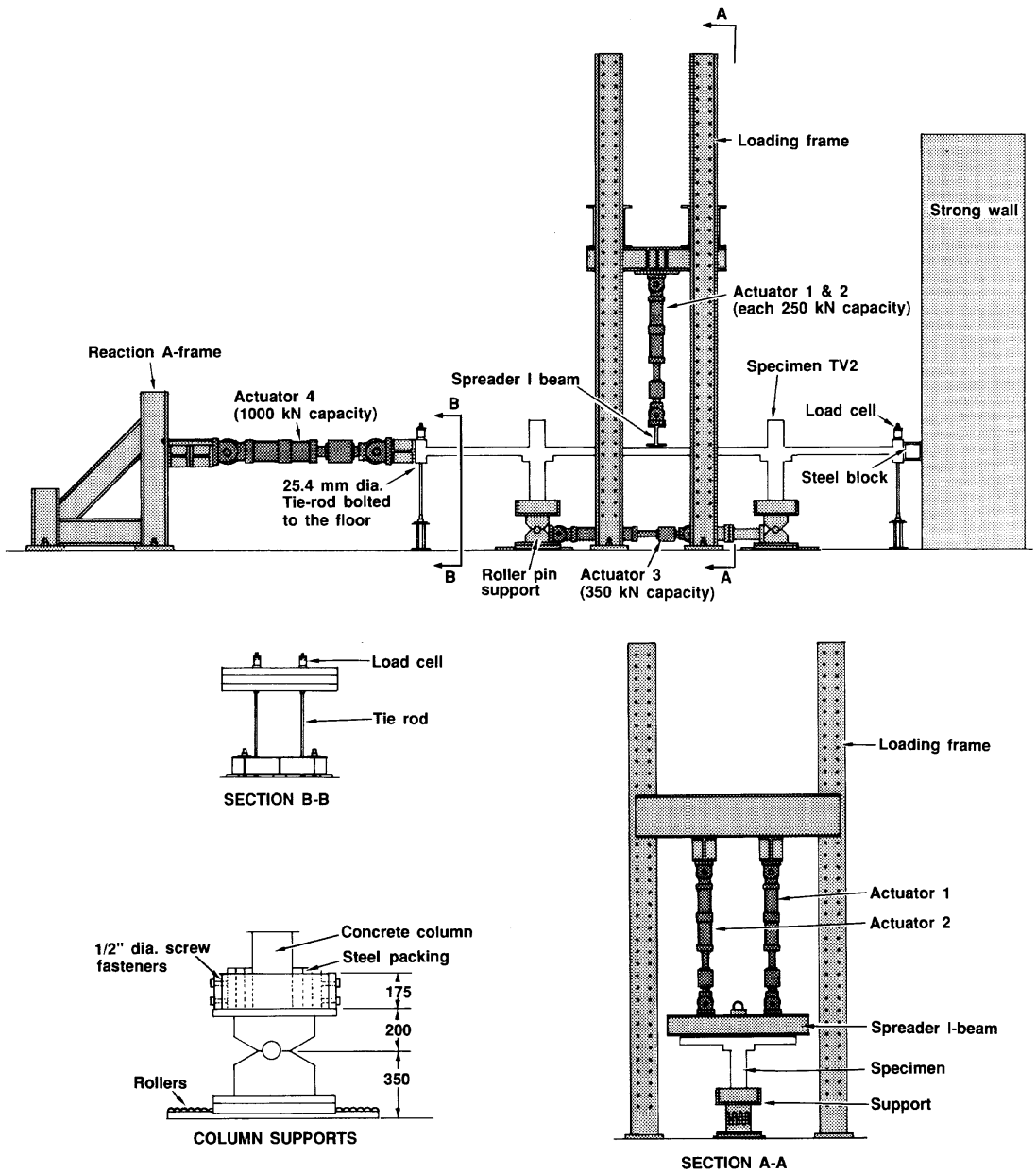

FIG. 5. Test setup.

of the specimen, an average axial strain of approximately 0.5×10^{-3} mm/mm was present in slab TV2 at ultimate load. Variations in the axial strain and curvature measured along the longitudinal axis of the slabs are represented in Fig. 8.

The reaction forces developed in the test specimens are described in Fig. 9. Figure 9*a* indicates the inward horizontal forces measured at the base of the columns. It would appear that these forces initially increased in direct proportion to the applied load. At near-ultimate conditions, the increase in restraint forces intensified. Also note that little difference is seen between these forces in the two specimens. The vertical reactions developed at the slab ends (i.e., at the tie-rods) are shown in Fig. 9*b*. Relatively small forces were induced initially, and were of similar levels in the two specimens. However, in slab TV2, these tie-down forces increased rapidly as the ultimate load condition was approached. The horizontal reaction force (i.e., membrane force) induced in slab TV2 is shown in Fig. 9*c*. Initially small, this force increased rapidly at intermediate load states. As the applied load on the specimen approached 85 kN, the induced membrane force reached 380 kN, i.e., almost 4.5 times the applied load. At ultimate load, the induced compression began to decrease. No corresponding force was present in slab TV1 because of the different support conditions.

The strains developed in the bottom reinforcement at the midspan and in the top reinforcement at the inside face of the columns are given in Fig. 10. Observe that at both locations, relatively higher strains were developed in the slab TV1 reinforcement. Yield strains were achieved in the bottom midspan reinforcement of both specimens, although at a considerably lower load in slab TV1. Also note that the effects of concrete cracking were more perceptible in the TV1 reinforcement

FIG. 6. Slab specimens after failure: (*a*) punching failure of slab TV1; (*b*) failure of slab TV2 due to rebar rupturing.

strains; the axial compression induced in slab TV2 resulted in a more gradual transition. In the top reinforcement at the column face, yielding was clearly achieved in slab TV2, whereas a stress of 375 MPa (0.82 f_y) only was attained in slab TV1 before the premature failure.

The cracking patterns developed in the test specimens indicated that the slab strips were essentially behaving in a one-way manner. The cracks on the underside of the slabs were perpendicular to the longitudinal direction, and ran full-width. Cracking on the top side of the slabs, near the columns, were

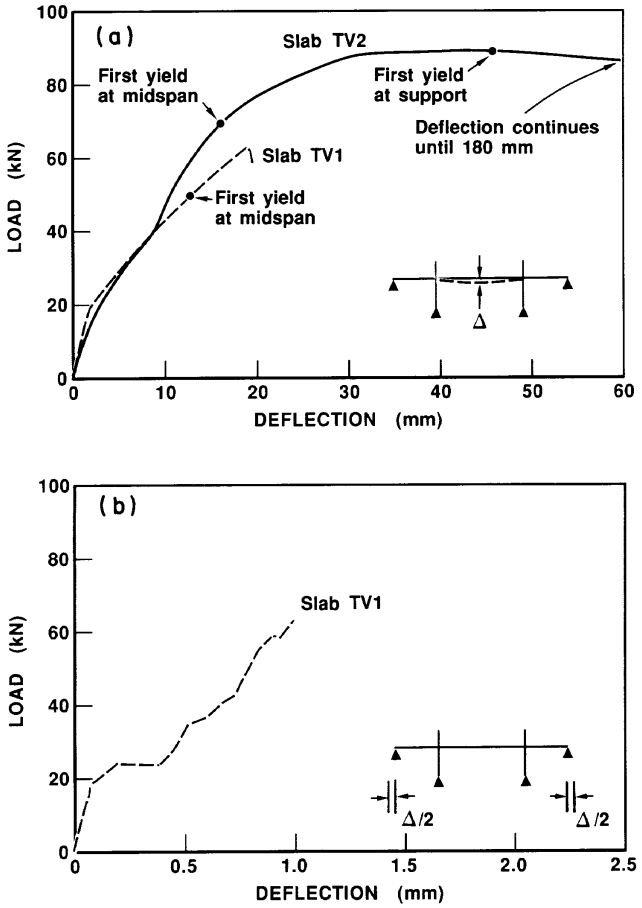

FIG. 7. Load–deformation response of test slabs: (*a*) slab deflection at midspan; (*b*) relative lateral displacement of slab ends.

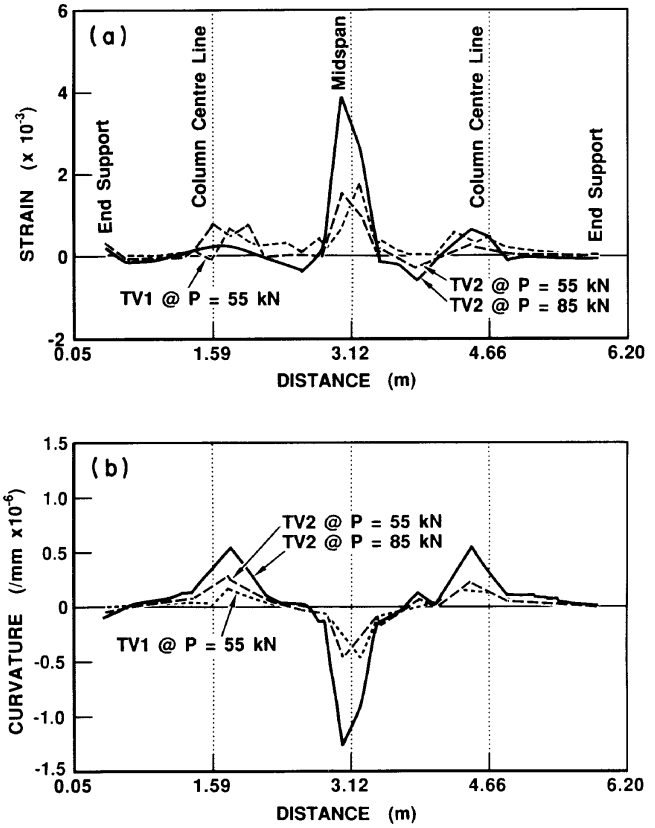

FIG. 8. Strain variations measured along longitudinal axes of slabs: (*a*) axial strain at mid-depth; (*b*) curvature.

initially of this nature as well. Only at advanced stages of loading did radial cracks develop around the columns. The crack patterns present just prior to failure, in each of the two specimens, are shown in Fig. 11.

Discussion

Slab TV2 demonstrated considerably greater strength and stiffness than did slab TV1. The enhanced response was brought on entirely by the development of compressive membrane action. High axial compressive forces were induced in slab TV2, primarily from the end restraint condition and to a much lesser extent from the lateral restraint offered by the columns. At ultimate load, the axial compression in the slab totalled 415 kN. In slab TV1, conversely, the axial compression developed through the lateral restraint of the columns amounted to only 15 kN just prior to failure. Shown in Fig. 12*a* are partial constructions of the axial load–moment interaction diagrams for the slab cross section at the midspan and column–joint regions. For an axial load of 15 kN, the nominal moment capacity at the midspan is seen to be 19.5 kN · m. At an axial load of 415 kN, the flexural resistance is increased by 80% to 35.1 kN · m. Similar increases in moment capacity can also be observed for the slab section at the column supports. These increased section capacities were directly responsible for the substantial enhancement in load capacity observed in slab TV2. Thus, membrane action was demonstrated to be an important second-order effect, significantly affecting slab deflections and load capacity.

The test results also indicated that geometric nonlinearity effects can significantly influence behaviour as well. Large deflections, coupled with high axial compressive forces, will result in large secondary moments owing to load eccentricity. These secondary moments detract from the load-carrying capacity of the structure. In slab TV2, the midspan deflection at ultimate load was approximately 40 mm. The 415 kN axial compressive force also present resulted in a secondary moment of 16.6 kN · m, which consumed about 20% of the flexural capacity (see Fig. 12*b*). This led to accelerated hinging at the midspan and a redistribution of forces within the structure. Ignoring this effect, but still allowing for the strength enhancement due to membrane forces, would result in a significant overprediction of load capacity.

Also worth noting once again is that catenary action was not an achievable condition. The No. 10 reinforcing bars used, the same grade as might be supplied to a construction site, fractured well before the axial compression in the slab was relieved.

Finally, it was interesting to note from the crack and deflection patterns that slab behaviour was essentially one-way. All major flexural cracks remained perpendicular to the longitudinal axis of the slab and ran full-width. Only at advanced stages of loading did radial cracks begin to form around the columns. At ultimate, yielding of the top reinforcing bars was experienced across the full width of the slab strip at the columns.

Theoretical response

Theoretical predictions of the response of the test specimens were made using program TEMPEST (Vecchio 1987), a computer code for the nonlinear structural analysis of reinforced

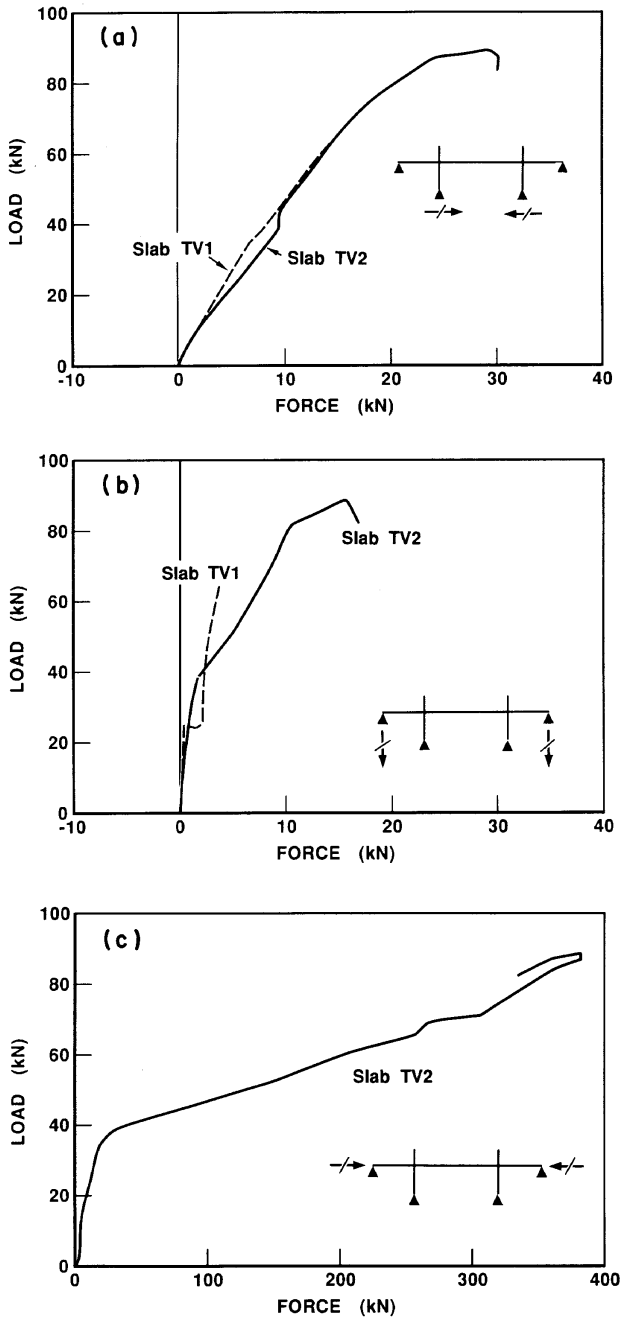

FIG. 9. Restraint forces developed in test slabs: (*a*) lateral reaction at column base; (*b*) vertical reaction at slab ends; (*c*) lateral reaction at slab ends.

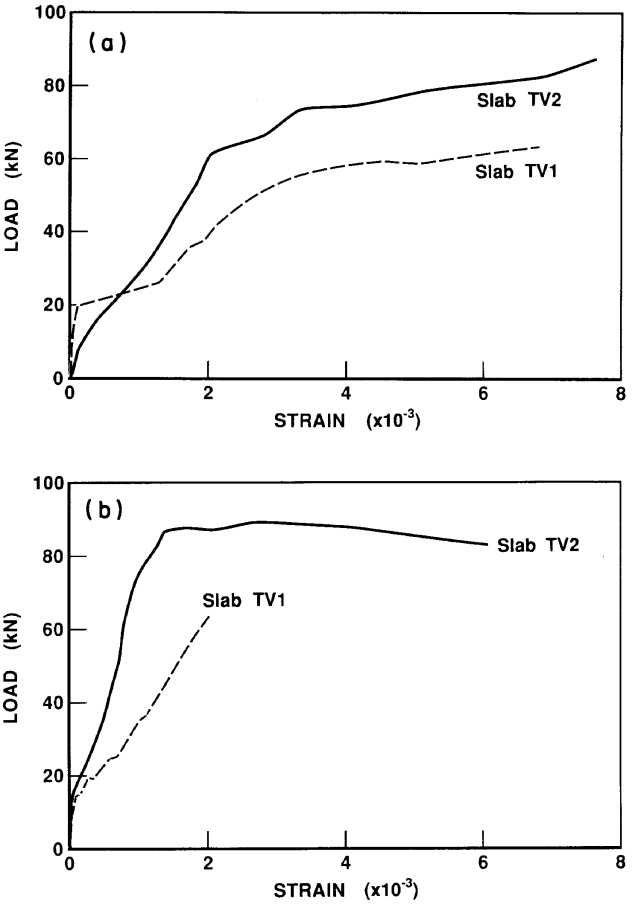

FIG. 10. Rebar strains measured in test slabs: (*a*) strain in bottom rebar at midspan; (*b*) strain in top rebar at column inside face.

concrete plane frames. The analytical procedure is essentially based on a total load, iterative, secant stiffness algorithm using layered sectional analysis methods. Its formulations incorporate appropriate nonlinear constitutive relations for the concrete and the reinforcement, and allow for the consideration of geometric nonlinearity, membrane action, tension stiffening effects, strain hardening, and other second-order influences.

To perform an analysis of the slab strip specimens, the test structure had to be modelled as a plane frame. Recognizing the symmetry of both the structure and the load conditions, only half the structure was considered. Shown in Fig. 13 is the computer model used, indicating the discretization of members and the definition of member cross sections. The same model was used for both slabs TV1 and TV2, with the only difference being the horizontal support condition imposed at the slab end. The horizontal end displacement was fixed for slab TV2, but left free for slab TV1. For both slabs, the vertical member at the slab end, representing the tie-rods, was modelled using a spring element with an axial stiffness equivalent to that observed in the test response. The material strengths used corresponded to those measured in the test specimen. A parabolic compressive stress–strain curve was used for concrete. The curvilinear stress–strain response of the No. 10 longitudinal bars was modelled using a bilinear curve with a yield strength of 450 MPa and a strain-hardening modulus of 2000 MPa.

Shown in Fig. 14*a* is the predicted response for slab TV1 in terms of load versus midspan deflection. The theoretical response is seen to have an initial stiffness equivalent to that observed experimentally. After cracking, however, the predicted load–deformation response is somewhat stiffer. First yielding at the midspan is predicted to occur at a load of between 45 and 50 kN; the experimentally observed yield load was 50 kN. A ductile failure is predicted with hinging at the midspan and inside face of the column supports. The theoretical ultimate load capacity is predicted to be 70 kN, with no enhancement possible through catenary action. Slab TV1 failed suddenly and prematurely, due to equipment malfunction, at 90% of the theoretical ultimate load.

The theoretical and experimental load–deformation responses for slab TV2 are compared in Fig. 14*b*. The predicted response is again somewhat stiffer than the observed

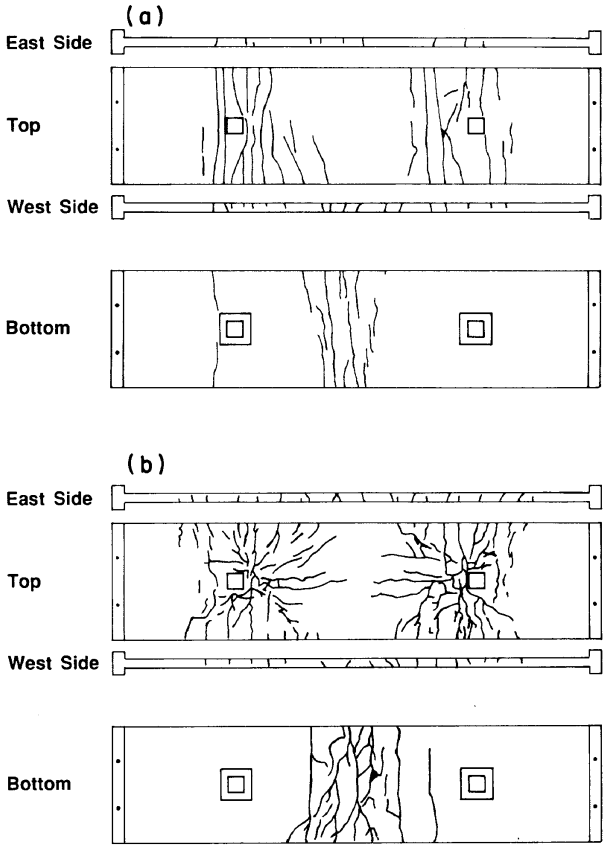

FIG. 11. Slab crack patterns: (*a*) slab TV1 at load of 58 kN; (*b*) slab TV2 at load of 84 kN.

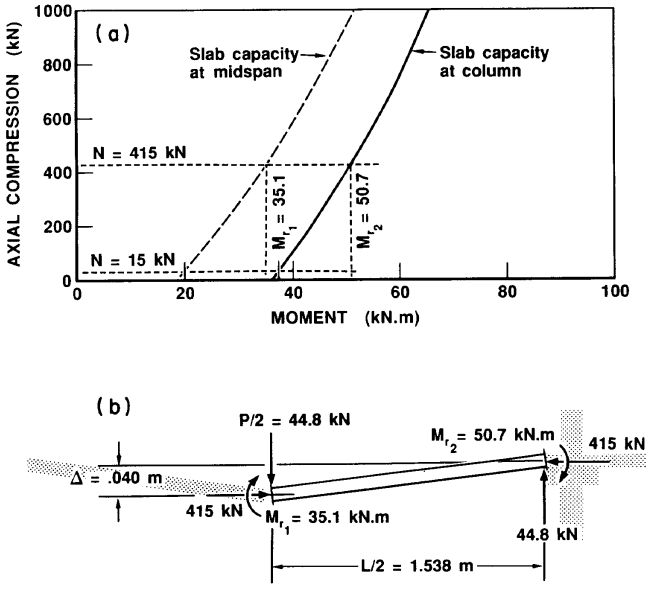

FIG. 12. Moment–axial load interaction diagram for slab section: (*a*) moment–axial load interaction diagrams; (*b*) equilibrium condition in slab TV2 at ultimate load.

behaviour. First yielding is predicted to occur at 70 kN load, corresponding well to the observed yield load of 74 kN. The theoretical ultimate load is 100 kN, with failure again occurring by means of a three-hinge mechanism. The experimen-

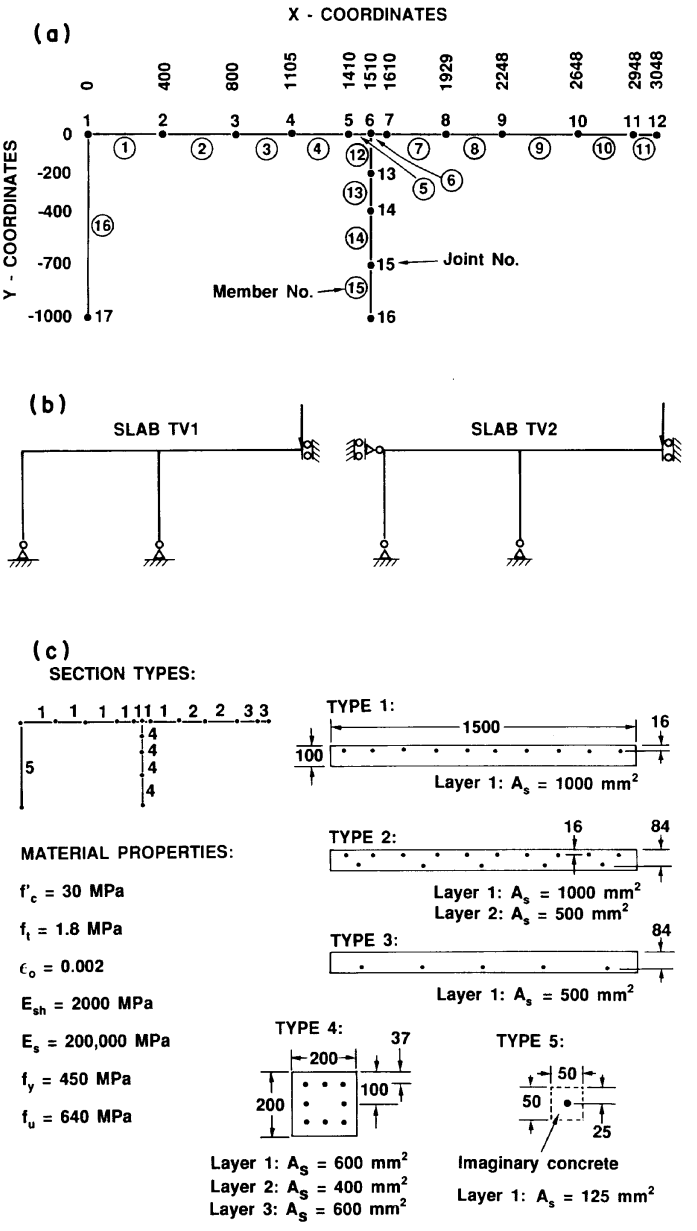

FIG. 13. Computer analysis model of test specimens: (*a*) discretization of members; (*b*) support conditions; (*c*) section properties.

tally observed failure load was 89.4 kN, or 89% of the theoretical value. Note that very ductile post-ultimate behaviour is seen in both the experimental and theoretical response curves. In both cases, ultimate load capacity is reached when the slab deflection approaches 50 mm, i.e., one-half the slab thickness.

Other aspects of response were also examined and found to be predicted reasonably well. Compared in Fig. 15 are the predicted and observed reaction forces in slab TV2. The column lateral reaction force (Fig. 15*a*) and the slab-end vertical reaction force (Fig. 15*b*) are well predicted. These forces are somewhat dependent on relative stiffness changes throughout the structure, but primarily on first-order moment distribution. Good agreement here is expected. However, the lateral reaction at the slab end, shown in Fig. 15*c*, is entirely dependent on second-order nonlinear effects, and thus is much more difficult to accurately predict. That reasonably good agree-

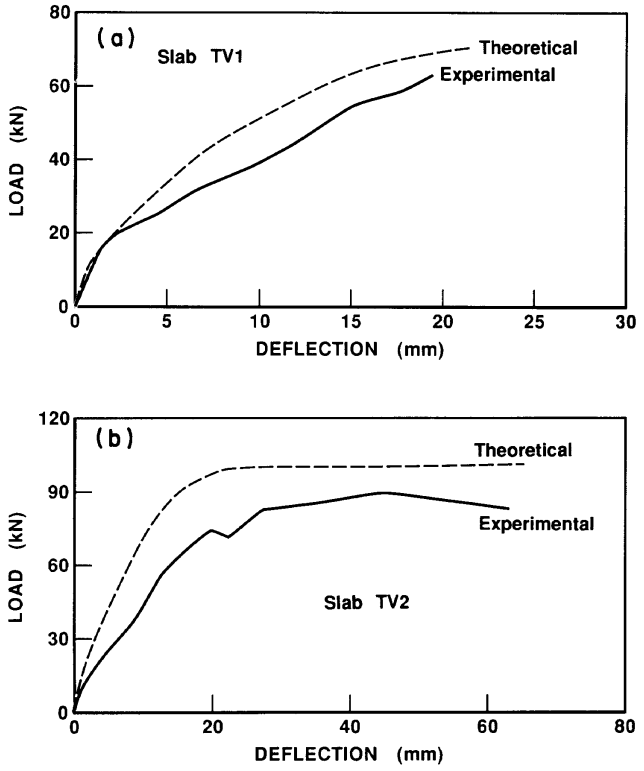

FIG. 14. Comparison of theoretical versus experimental load–deformation response: (*a*) midspan deflection of slab TV1; (*b*) midspan deflection of slab TV2.

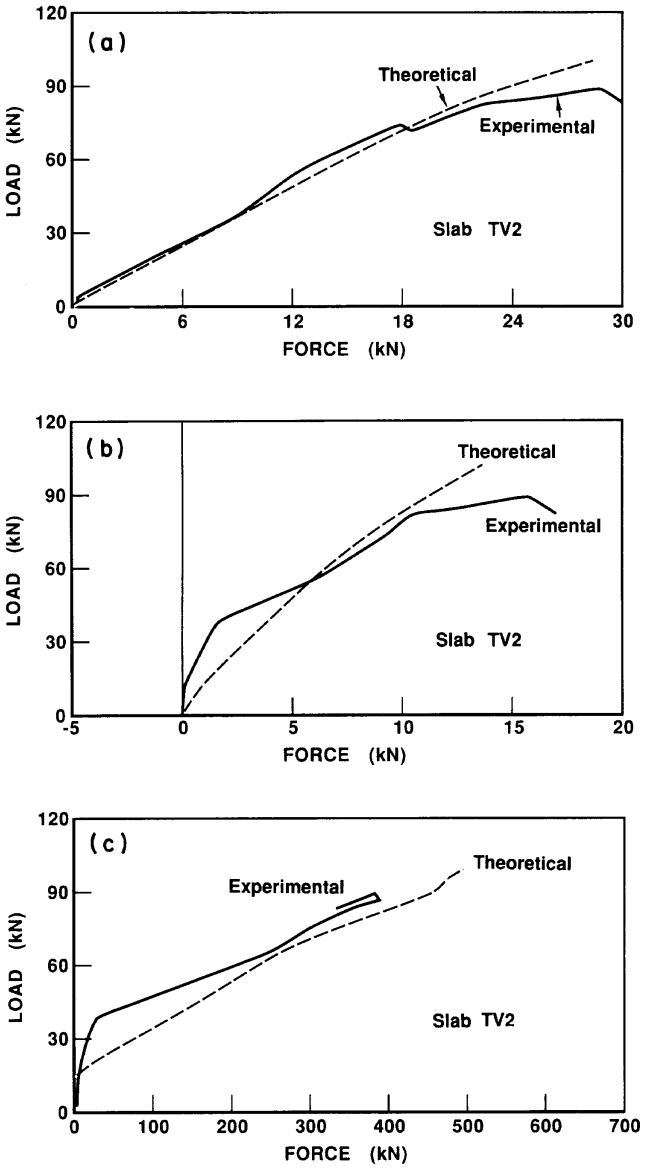

FIG. 15. Comparison of theoretical versus experimental restraint forces: (*a*) lateral reaction at column base; (*b*) vertical reaction at slab end; (*c*) lateral reaction at slab ends.

ment is seen here is much more significant. Predictions of comparable accuracy were also obtained for displacements and rebar strains, at monitored locations, for both test specimens.

In general, the theoretical analyses provided a reasonably accurate description of the test specimen behaviour. The tendency to slightly overestimate strength and stiffness is likely related to the influence of two-way action around the column supports. Modelling the structures as plane frames is equivalent to assuming a line support at the column locations, a more favourable condition than actually existed. Improved modelling of the test specimens could be accomplished through the use of an appropriate nonlinear finite element shell analysis program.

The ultimate load capacity of the slabs can be estimated using simple plastic analysis techniques. A plastic analysis for slab TV1, assuming plastic hinges at the midspan and column supports and no axial load in the slab, would result in an ultimate load prediction of 70 kN. This is equivalent to the capacity predicted by the nonlinear frame analysis. A similar analysis for slab TV2, but assuming zero strain at the slab mid-depth, results in an ultimate load prediction of 151 kN with a corresponding axial load of 1400 kN. This predicted capacity is 67% greater than the observed failure load and 50% greater than that predicted by the nonlinear frame analysis. In essence, it ignores the influences of geometry nonlinearity.

Christiansen's method for predicting ultimate load, applied to the conditions of the fully restrained test slab, results in a predicted capacity of 100 kN. This is identical to the value obtained from the nonlinear frame analysis and 10% higher than the experimental result. The formulations proposed by Park and by Brotchie and Holley are intended for rectangular two-way concrete slabs under uniformly distributed loading. As such, they are not applicable here.

Conclusions

The results of the experimental program were a clear demonstration of the influence of membrane action in reinforced concrete slabs. In a laterally restrained slab, the axial forces induced were several times larger than the applied load. These axial forces served to increase the flexural stiffness and load-carrying capacity of the slab by about 30–40% relative to an unrestrained slab. The test results also indicated that geometric nonlinearity effects also had a significant influence on capacity. The high axial forces induced, coupled with large slab deflections at ultimate load, created large secondary moments which partially negated the beneficial influences of membrane action.

The nonlinear plane frame analysis procedure used to predict the behaviour of the test specimens was shown to

accurately represent the complex second-order effects. The load–deformation response of the slabs, the pattern of internal forces and strains, and the ultimate load capacity were all predicted reasonably well. The tendency to slightly overestimate strength and stiffness was likely the result of an inability to consider two-way slab behaviour around the columns.

The test results suggest that a reasonably accurate assessment was made of the ultimate load capacity of the Kimberley–Clark Warehouse floor. The beneficial effects of two-way action in a slab supported along all four sides would likely offset any overestimate of strength as seen in the slab strips tested.

Current research work is aimed at developing nonlinear finite element analysis procedures for plates and shells, which can adequately model important second-order effects. Efforts are also being made at improving the constitutive modelling of the materials.

Acknowledgement

The work described in this paper was made possible through funding from the Natural Sciences and Engineering Research Council of Canada. The authors wish to express their gratitude for the support received.

BROTCHIE, J. F., and HOLLEY, M. J. 1971. Membrane action in slabs. American Concrete Institute Publication SP-30-16, pp. 345–355.

CHRISTIANSEN, K. P. 1963. The effect of membrane stresses on the ultimate strength of the interior panel in a reinforced concrete slab. The Structural Engineer (London), **41**(8): 261–265.

GUICE, L. K., and RHOMBERG, E. J. 1988. Membrane action in partially restrained slabs. American Concrete Institute Structural Journal, **85**(4): 365–373.

HEWITT, B. E., and BATCHELOR, B. DEV. 1975. Punching shear strength of restrained slabs. ASCE Journal of the Structural Division, **101**(ST9): 1837–1853.

HOPKINS, D. C., and PARK, R. 1971. Test on a reinforced concrete slab and beam floor designed with allowance for membrane action. American Concrete Institute Publication SP-30-10, pp. 223–234.

JOHANSEN, K. W. 1962. Yield-line theory. Cement and Concrete Association, London, United Kingdom.

KINNUNNEN, S., and NYLANDER, H. 1960. Punching of concrete slabs without shear reinforcement. Transactions of the Royal Institute of Technology, Stockholm, Sweden, No. 158.

OCKELSTON, A. J. 1955. Load tests on a three-storey reinforced concrete building in Johannesburg. The Structural Engineer (London), **33**(10).

PARK, R. 1964. Ultimate strength of rectangular concrete slabs under short term uniform loading with edges restrained against lateral movement. Proceedings, Institution of Civil Engineers (London), **28**: 125–150.

——— 1965. The lateral stiffness and strength required to ensure membrane action at the ultimate load of a reinforced concrete slab and beam floor. Magazine of Concrete Research (London), **17**(50): 29–38.

VECCHIO, F. J. 1987. Nonlinear analysis of reinforced concrete frames subjected to thermal and mechanical loads. American Concrete Institute Structural Journal, **84**: 492–501.

VECCHIO, F. J., and COLLINS, M. P. 1990. Investigating the collapse of a warehouse. Concrete International, **12**(3): 72–78.

WESTERGAARD, H. M., and SLATER, W. A. 1921. Moments and stresses in slabs. American Concrete Institute Journal, **17**: 415–538.

List of symbols

A_s cross-sectional area of reinforcement bar
f'_c concrete cylinder compressive strength
f_{ct} concrete split cylinder cracking strength
f_u rebar steel ultimate strength
f_y rebar steel yield stress
E_c modulus of elasticity of concrete (initial tangent value)
E_s modulus of elasticity of rebar steel
ε_0 concrete cylinder strain at peak compressive stress